

1 **SARS-CoV-2 Delta variant induces enhanced pathology and inflammatory responses in**
2 **K18-hACE2 mice**

3
4 Katherine S. Lee^{1,2}, Ting Y. Wong^{1,2}, Brynnan P. Russ^{1,2}, Alexander M. Horspool^{1,2}, Olivia A.
5 Miller^{1,2}, Nathaniel A. Rader^{1,2}, Jerome P. Givi³, Michael T. Winters¹, Zeriel YA. Wong¹, Holly A.
6 Cyphert⁴, James Denvir⁵, Peter Stolov⁶, Mariette Barbier^{1,2}, Nadia R. Roan^{7,8}, Md. Shahrier
7 Amin³, Ivan Martinez^{1,9}, Justin R. Bevere^{1,2} and F. Heath Damron^{1,2*}

8
9 ¹ Department of Microbiology, Immunology, and Cell Biology, West Virginia University,
10 Morgantown, WV, USA

11 ² Vaccine Development Center at West Virginia University Health Sciences Center,
12 Morgantown, WV, USA

13 ³ Department of Pathology, Anatomy, and Laboratory Medicine, West Virginia University,
14 Morgantown, WV, USA

15 ⁴ Department of Biological Sciences, Marshall University, Huntington, WV, USA

16 ⁵ Department of Biomedical Sciences, Marshall University, Huntington, WV, USA

17 ⁶ Department of Biochemistry, School of Medicine, West Virginia University Morgantown, WV,
18 USA

19 ⁷ Department of Urology, University of California, San Francisco, San Francisco, CA, USA

20 ⁸ Gladstone Institute of Virology, San Francisco, CA, USA

21 ⁹ West Virginia University Cancer Institute, School of Medicine, Morgantown, WV, USA

22

23 * Corresponding author

24 Corresponding author email address: fdamron@hsc.wvu.edu

25

26 Keywords: SARS-CoV-2, COVID-19, K18-hACE2 transgenic mouse, WA-1 variant, alpha
27 variant, beta variant, delta variant, RNAseq, COVID-19 histopathology

28

29 **Abstract**

30 The COVID-19 pandemic has been fueled by novel variants of concern (VOC) that have
31 increased transmissibility, receptor binding affinity, and other properties that enhance disease.
32 The goal of this study is to characterize unique pathogenesis of the Delta VOC strain in the K18-
33 hACE2-mouse challenge model. Challenge studies suggested that the lethal dose of Delta was
34 higher than Alpha or Beta strains. To characterize the differences in the Delta strain's
35 pathogenesis, a time-course experiment was performed to evaluate the overall host response to
36 Alpha or Delta variant challenge. qRT-PCR analysis of Alpha- or Delta- challenged mice
37 revealed no significant difference between viral RNA burden in the lung, nasal wash or brain.
38 However, histopathological analysis revealed high lung tissue inflammation and cell infiltration
39 following Delta- but not Alpha-challenge at day 6. Additionally, pro-inflammatory cytokines were
40 highest at day 6 in Delta-challenged mice suggesting enhanced pneumonia. Total RNA-
41 sequencing analysis of lungs comparing infected to uninfected mice revealed that Alpha-
42 challenged mice have more total genes differentially activated, conversely, Delta-challenged
43 mice have a higher magnitude of differential gene expression. Delta-challenged mice have
44 increased interferon-dependent gene expression and IFN- γ production compared to Alpha.
45 Analysis of TCR clonotypes suggested that Delta challenged mice have increased T-cell
46 infiltration compared to Alpha challenged. Our data suggest that Delta has evolved to engage
47 interferon responses in a manner that may enhance pathogenesis. The *in vivo* and *in silico*
48 observations of this study underscore the need to conduct experiments with VOC strains to best
49 model COVID-19 when evaluating therapeutics and vaccines.

50

51

52 **Importance**

53 The Delta variant of SARS-CoV-2 is known to be more transmissible and cause severe disease
54 in human hosts due to mutations in its genome that are divergent from previous variants of
55 concern (VOC). Our study evaluates the pathogenesis of Delta in the K18-hACE2 mouse model
56 compared to the Alpha VOC. We observed that relative to Alpha, Delta challenge results in
57 enhanced inflammation and tissue damage with stronger antiviral responses. These
58 observations provide insight into Delta's unique pathogenesis.

59

60 **Introduction**

61 The COVID-19 pandemic is being perpetuated by the emergence of “Variants of Concern”
62 (VOC), mutant strains of SARS-COV-2 with enhanced disease-causing abilities. Early in the
63 pandemic, strains obtained the D614G mutation that enhanced binding of the spike protein to
64 the host hACE2 receptor. The mutation quickly became dominant in the circulating strains
65 around the world. Several potential variant strains were noted and monitored but few
66 demonstrated any unique or enhanced differences in virulence or transmission. In September
67 2020, the B.1.1.7 strain was first identified in the United Kingdom and quickly spread to become
68 the dominant variant worldwide in early 2021 (1). Later, in December 2020, two other variants,
69 Beta (B.1.351) and Gamma (P.1) were identified in South Africa and Japan/Brazil, respectively
70 (2–4). Both Beta and Gamma increased concerns because they decreased efficacy of several
71 vaccines in clinical trials (4–10).

72 In addition to the effects on vaccine efficacy in clinical trials, there were also reports that Alpha
73 and Beta variants were able to cause enhanced disease in humans (11–16) and animal studies
74 with transgenic K18-hACE2-mice and hamsters supported those observations (17,18). Before
75 circulating VOC established their dominance, two doses of Pfizer-BioNTech's mRNA vaccine,
76 BNT162b2, exhibited 95% efficacy in protecting individuals from severe COVID-19 in
77 retrospective cohort studies of COVID-19-associated hospitalizations in early 2021 (19).

78 However, the efficacy of the BNT162b2 vaccine was slightly diminished in the context of the
79 Alpha (93.7% efficacy) (20).

80 As Alpha, Beta, and Gamma continued to spread, the Delta variant (B.1.617.2) was identified in
81 India, resulting in a massive surge of COVID-19 cases in the country (21). Unsurprisingly, Delta
82 was able to cause breakthrough cases of infection within a portion of fully vaccinated people,
83 decreasing the overall efficacy of ChAdOx1, mRNA-1273, or BNT162b2 vaccines (20,22–24). In
84 March 2021, the Delta variant was detected in the United States, and reports of its increased
85 transmissibility necessitated investigation of its threat to both unvaccinated and vaccinated
86 populations. Key pathogenic mutations in the B.1.617 SARS-CoV-2 lineage, which includes the
87 Delta (B.1.617.2) and Kappa (B.1.617.1) VOC, occur within the spike protein, which mediates
88 viral attachment and entry into host cells via the ACE2 receptor (25,26). These mutations have
89 been reported to increase transmissibility within the population and decrease antibody
90 neutralization (27). Delta does not harbor the N501Y substitution in the spike protein that was
91 characteristic of the Alpha and Beta lineages but Delta does harbor the D614G substitution in
92 spike, which contributes to the increased fitness and transmissibility of many VOC strains
93 (28,29). Some strains of Delta are reported to harbor the K417N mutation previously found in
94 Beta and Gamma, which sparked debate over designating the strain as a new variant (30,31).
95 This mutant strain was labeled as “Delta Plus.” Additional mutations within the spike protein of
96 Delta include P681R, which diverge from other VOC and help to enhance ACE2 receptor
97 binding and cellular entry, contributing to reported increases in Delta’s pathogenicity (32).

98 To characterize the pathogenicity of Delta (utilizing strain B.1.617.2) and how it diverges from
99 prior VOC (WA-1, Alpha, and Beta strains), we performed a time-course challenge study in K18-
100 hACE2 transgenic mice, which were intranasally challenged with Alpha and Delta strains.
101 Through analysis of viral load, tissue pathology, cytokine profiling, and total transcriptomics of
102 the lung, we discovered that Delta causes increased interferon type I and II responses

103 corresponding with greater lung inflammation when compared to Alpha. These data help to
104 advance pre-clinical models of COVID-19 as well as serve as a benchmark to compare past and
105 future VOC strains.

106

107 **Results**

108 **The Delta Variant of SARS-CoV-2 has a greater LD100 than Alpha and Beta VOCs in K18-
109 hACE2 mice.** To date, most K18-hACE2 mouse or Golden Syrian hamster studies have
110 utilized ancestral viral strains of SARS-CoV-2 (e.g., WA-1, D614G, B.1 Wuhan), and few studies
111 have been performed with emergent VOC (2,17,18,33–39). Early studies in K18-hACE-mice
112 with a variety of viral strains used a wide range of challenge doses from as low as 100 PFU to
113 as high as 10^5 PFU (40–42). In pilot studies with the Alpha and Beta variants, we evaluated 10^5
114 PFU (high dose) and observed mortality as early as day 4 post challenge, suggesting that VOCs
115 have enhanced virulence in K18-hACE-mice compared to WA-1 ancestral strain (data not
116 shown). We then aimed to identify an appropriate challenge dose for WA-1, Alpha, Beta, and
117 Delta VOC that could cause symptomatic disease for appropriate comparisons between the
118 subtle aspects of variant pathogenicity masked by lethal challenge doses. At the low dose of 10^3
119 PFU, WA-1 challenge only resulted in morbidity of 50% of the mice (Fig. 1A). We observed that
120 a challenge dose of 10^3 PFU using Alpha or Beta resulted in 80% and 100% mortality,
121 respectively by day 7 post challenge. Although this comparison between Alpha and Beta
122 challenge at 10^3 PFU is not statistically significant ($P= 0.6452$), there is a significant difference
123 between the survival of WA-1 challenged mice compared to Beta at the 10^3 PFU dose, where
124 WA-1 elicits higher survival ($P= 0.0446$). Despite the observations of enhanced virulence of
125 Delta in humans, 10^3 PFU challenge of K18-hACE2-mice mirrored WA-1 survival more so than
126 Alpha or Beta (Fig. 1A). As expected, increasing the challenge dose to 10^4 PFU decreased
127 survival of K18-hACE2-mice for all strains (Fig. 1B). At the 10^4 PFU challenge dose, Delta
128 resulted in 0% survival (Delta vs WA-1 $P= 0.0002$) (Fig. 1A-B). The 10^4 PFU challenge dose

129 also shortened the time to morbidity for Beta as well as Alpha (WA-1 vs Alpha $P=0.0008$; WA-1
130 vs Beta $P=0.0122$). As we suspected from an ancestral strain, total morbidity of WA-1 infected
131 groups was not observed at the either dose. Using a disease scoring system established
132 previously (T.Y.Wong, K. S. Lee, et al., JVI accepted for publication) we observed higher
133 average disease scores for Alpha and Beta than Delta in K18-hACE2 mice intranasally
134 challenged with 10^3 PFU (Alpha vs Delta $P=0.0355$; Beta vs Delta $P=0.0039$) (Fig. 1C-D).
135 Interestingly, Delta's observable disease phenotypes remained low by day 6 when Alpha- and
136 Beta- challenged mice started to develop greater observable disease phenotypes consistent
137 with morbidity (Alpha vs Delta $P=0.0056$). Delta's disease phenotypes were scored higher
138 following 10^4 PFU challenge, where they progressed in a pattern similar to Alpha. Delta-
139 challenged mice received higher average disease scores than Beta by day 6 post challenge
140 (Fig. 1D). These experiments suggested that Delta compared to WA-1, Alpha, and Beta We
141 reasoned that these differences warranted further investigation.

142 **Mice challenged with of Alpha or Delta experience unique disease manifestation.** To gain
143 additional insights into the differences in pathogenesis of Alpha and Delta in K18 mice, we
144 focused on a challenge dose of 10^3 PFU which allows for differential disease manifestation
145 between Alpha and Delta. Rectal temperature and weight loss were monitored in mice
146 challenged with 10^3 PFU of Alpha or Delta. In agreement with their disease scores, Alpha
147 challenged mice had significant loss of body temperature (hypothermia) and weight loss
148 between days 5 and 6 post challenge (Fig. 1E-F). However, Delta-challenged mice maintained
149 body temperature and did not experience weight loss (Fig. 1G-H). At day 6 post challenge,
150 Alpha challenged mice had reached morbidity based on disease scoring and required
151 euthanasia as a humane endpoint. However, at day 6 Delta challenged mice remained below
152 euthanasia criteria. Collectively, these data demonstrate that Alpha and Delta cause distinct
153 disease profiles in K18-hACE2-mice.

154 **Mice challenged with Delta have similar levels of viral RNA burden in the nares, and**
155 **lungs but lower amounts of viral RNA in the brain.** It has been previously reported that
156 SARS-CoV-2 viral burden is highest two days after challenge (43) and based on our data we
157 recognize that Alpha variant will cause morbidity at day 6 post-challenge; however, Delta variant
158 challenge will not cause the same disease, or survival. Therefore, we aimed to evaluate viral
159 RNA burden at day 2 and 6 post challenge for Alpha or Delta challenge mice. At euthanasia on
160 day 2 and 6 the lung, brain, and nasal wash fluid were collected from challenged mice to
161 quantify viral RNA burden via nucleocapsid qRT-PCR. We observed that viral RNA burden was
162 remarkably similar between Alpha and Delta in the lung at both time points (Fig. 2A). In the
163 nasal wash, viral load was also detectable at similar levels for both Alpha and Delta at day 2. In
164 contrast to the lung, the viral RNA burden decreased to undetectable levels at day 6 for both
165 VOC (Fig. 2B). Surprisingly, challenge with Delta did not lead to detectable levels of viral RNA in
166 the brain at either day 2 or day 6. In contrast, mice infected with Alpha exhibited low RNA levels
167 at day 2 and a 2-fold increase at day 6, suggesting viral replication in the brain over time (Fig.
168 2C). These observations suggest that Delta replicates efficiently in the airway in a manner
169 similar to Alpha but Delta appears to lack the brain localization previously observed in K18-
170 hACE2 mice (43–46).

171 **Mice challenged with Delta experience significant inflammation in the lung tissue.** Based
172 on qRT-PCR data showing viral RNA burden in the lung but not brain of 10^3 PFU Delta-
173 challenged mice, we hypothesized that relative to other Alpha, Delta may cause robust
174 pneumonia and less encephalitis in K18-hACE2-mice. To test this, we performed
175 histopathological analysis on the lungs collected at days 2 and 6 to characterize the pneumonia
176 caused by Alpha or Delta challenge. At two days following challenge, inflammation, and
177 recruitment of inflammatory cells could already be observed in the Delta- but not Alpha-
178 challenged mice when compared to the lungs of uninfected mice (Fig. 3A-B). At this time, a

179 pathologist identified that the inflammatory infiltrate was composed predominantly of
180 lymphocytes and occasional histiocytes. By day 6, an increase in marked perivascular
181 inflammation and margination was measured in Delta- (36.86 marginating lymphocytes per mm
182 length of endothelium) and Alpha-challenged mice (12.19 marginating lymphocytes per mm
183 length of endothelium) (unpaired t-test $P=0.026$) (Fig 3C-D). In Alpha lungs, less total vessels
184 were identifiable within areas of inflammation, awarding these samples a margination score of
185 zero cells/mm of vessel. Overall, less inflammation occurred in Alpha lungs. At day 6, only 1%
186 of the lung area featured inflammation in Alpha, compared to 20% for Delta-challenged mice
187 (unpaired t-test $P=0.003$) (Fig 3E). Within these tissue areas (the airway, alveoli, and thin
188 mucous layer), the presence of Delta virions was identified using electron microscopy (Fig 3F-
189 G). Collectively, these data suggest Delta challenged mice have increased cellular responses
190 and inflammation compared to Alpha challenged K18-hACE-mice.

191 **Pro-inflammatory cytokines are increased in mice challenged with Delta at day 6.**
192 Histopathological analysis revealed significant inflammation in the lungs of Delta-challenged
193 mice at day 6 compared to Alpha-challenged mice despite equal viral RNA burden. To better
194 understand differences in the inflammatory profile of these tissues, pro-inflammatory cytokine
195 levels in lung supernatant at day 2 or 6 were quantified to profile strain specific variations in the
196 “cytokine storm” (47). Insignificant amounts of cytokine were produced in the lungs of mice
197 challenged with Alpha or Delta at day 2 (Fig. 4). Alpha-challenged mice produced low amounts
198 of IL-1 β and CXCL13 compared to uninfected mice at day 2 or 6. By contrast, the cytokine
199 response to Delta challenge at day 6 compared to uninfected revealed high levels of IL-1 β ,
200 TNF α , and CXCL10 ($P=0.0462$, $P=0.0268$, $P=0.009$) (Fig. 4). The inflammatory response within
201 the lungs of mice challenged with Delta was elevated compared to Alpha. To gain insight into
202 the specific mechanisms of the immunological host response, we performed RNAseq to
203 characterize the total transcriptional profile of Alpha and Delta challenged K18-hACE2 mouse
204 lungs.

205 **RNAseq analysis of lung tissues from mice challenged with Alpha or Delta shows no**
206 **difference in viral sgRNA.** We utilized RNA that was isolated from the lung tissue of
207 challenged and uninfected mice at 2- and 6-days post-challenge for Illumina transcriptomic
208 analysis. RNA sequencing reads were first mapped to the SARS-CoV-2 viral genome to quantify
209 the expression levels of viral genes over the course of infection (Fig. 5A). This revealed no
210 significant difference between the two strains (Fig. 5B-C) which directly supported the qRT-PCR
211 analysis (Fig. 2). It is known that SARS-CoV-2 infection results in down-regulation of hACE2
212 expression(48,49). Therefore, we mapped RNA reads to the hACE gene to analysis this effect.
213 Although not significant, a trend of lowered hACE2 expression occurred in Alpha challenged
214 mice, whereas Delta challenged mice appeared to experience only slightly reduced hACE2
215 expression (Fig. 5D). These observations together with qRT-PCR nucleocapsid data described
216 above, suggest that with equal viral burden (same challenge dose and equal viral RNA burden),
217 the differences in LD100 of Alpha and Delta as well as the disease phenotypes are likely related
218 to differences in host response to VOC and not overall viral load.

219 **Delta challenge causes a higher magnitude of host gene expression change compared to**
220 **Alpha.** To compare the host responses of Delta- and Alpha-challenged mice, we mapped lung
221 RNA sequencing reads to the mouse genome. We observed that Alpha or Delta challenge in
222 K18-hACE2 mice result in distinct transcriptional changes. Two days after challenge with Alpha,
223 2,413 statistically significant genes (FDR $P \leq 0.04$) were differentially expressed compared to
224 uninfected mice, a difference which increases more than two-fold to 5,664 genes at day 6. In
225 Delta groups, differential expression encompasses 3,048 and 4,489 genes respectively. Venn
226 diagrams of the gene sets comparing by variant and time-points illustrate overlaps in gene sets
227 that are either activated or repressed. Both activated and repressed gene sets increase from
228 day 2 to 6 (Fig. 6A). Further filtration of these sets of genes to identify those that are uniquely
229 affected by VOC challenge and timepoint revealed that Alpha challenge results in more genes
230 differentially regulated at day 6 than Delta challenge (Fig. 6B). A set of core-activated genes

231 was identified through a four-way comparison of VOC and timepoint. Alpha and Delta challenge
232 both activate a similar set of host genes despite their different disease pathology. After
233 identifying the commonalities in our data set, we sought to identify how host transcriptomics
234 differ between the groups. When the fold changes of this gene set were graphed on a curve
235 according to their respective values at 6 days post-Delta challenge, it became clear that
236 expression of these core genes follows a similar trend (Fig. 6C).

237 **GO analysis revealed unique systems of enriched genes in mice challenged with Delta.**
238 Gene Ontology (GO) term analysis was performed to systematically group transcriptomic
239 observations to identify specific pathways and gene systems whose expression changes in
240 response to Alpha and Delta challenge. Relative to Alpha-challenged mice, Delta-challenged
241 mice had a higher number of unique GO terms that were enriched at day 6 (Fig. 7A). To
242 categorize the specifically enriched terms in Delta at day 6, pathway enrichment ratios were
243 calculated for the top 30 GO terms (Fig. 7B). The expression of genes that were annotated with
244 GO terms pertaining to immune responses, anti-viral, or lymphocyte recruitment were
245 increased, as were genes of pathways associated with T cells and responses to IFN- β (Fig. 7B).
246 Due to the fact that GO term analysis identified T cell response genes to be enriched in Delta
247 challenged mice, we performed T cell receptor (TCR) clonotype analysis using RNAseq reads.
248 Within the uninfected mice, we detected ~50 total clonotypes. In Alpha-challenged mice, the
249 number of clones were decreased relative to uninfected at both day 2 and 6. By contrast, Delta-
250 challenged mice had decreased clones at day 2, but we observed a 6-fold increase in TCR
251 clones at day 6 (Fig. 7C). In counts of unique TCR clonotypes, the same trends were observed:
252 at day 6, Delta challenge had the most total unique TCR clones compared to non-challenged
253 mice, day 6 post-Alpha challenged mice, and day 2 post Delta challenged mice (Fig. 7D).
254 These data suggest that Delta may induce more robust T cell response.

255 **Delta challenge causes increases interferon dependent gene expression.** Gene expression
256 analysis focused by GO terms revealed Delta challenge induced expression of interferon

257 response genes (Fig. 7). Interferon is an import regulator of the antiviral response in humans.
258 It's variable expression in response to specific variants exemplifies the differences in the host
259 response. TGTP1 and IFI211, two interferon related genes, are the highest-expressed genes in
260 Delta at day 6 at a fold change of 52,725 or 11,733 higher than in uninfected mice. In Alpha at
261 day 6 these genes are 3,367 and 591-fold higher than uninfected. Due to the important role of
262 interferons in the anti-viral response to SARS-CoV-2 which may be differentially engaged by
263 VOC, we continued to compare the top 20 genes involved in general interferon responses. Total
264 gene counts in lung RNA from each experimental group are shown in Fig. 8A. Delta day 6
265 shows high interferon dependent gene expression as well as the highest fold change difference
266 (Fig. 8B). Collectively, these data suggest Delta challenge results in higher interferon response.
267 To test that hypothesis, we directly measured type I and II interferons in lung supernatants and
268 serum. Modest IFN- α or IFN- β were observed in both lung and serum (IFN- α : $P=0.0012$ Delta
269 day 6 vs No Challenge in lung supernatant; IFN- β : $P=0.0474$ Alpha Day 2 vs No Challenge in
270 serum); however, Delta challenge resulted in high IFN- γ at day 6 ($P=0.0265$ in lung supernatant,
271 $P=0.0103$ in serum compared to no challenge) (Fig. 8C-D).

272

273 **Discussion**

274 In this study, we modeled the pathogenesis of SARS-CoV-2 variants of concern in the K18-
275 hACE2 mouse challenge model. Based on our observations that the Delta variant differs in
276 disease manifestation from Alpha and Beta VOC-challenge, we performed an experiment to
277 compare Alpha- and Delta-challenged mice at disease-significant timepoints. Despite a similar
278 viral RNA burden in the respiratory tract at day 2 and 6, Delta causes more significant
279 inflammation in the lungs than Alpha as infection progresses. The host response also varies
280 over time, with Delta causing increased antiviral cytokine production, specifically IFN- γ , at day 6.
281 GO term analysis of Delta-challenged mice suggested a greater number of immunological

282 pathways that are implicated in the variant's pathogenesis compared to Alpha, further indicating
283 the unique nature of host response to individual variants.

284 Severe COVID-19 is perpetuated by dysregulated production of pro-inflammatory cytokines,
285 including type I and II interferons, in a "cytokine storm" pathology (47,50,51). Interferon-
286 stimulated genes (ISG) in patient lung tissues implicate the role of interferon in SARS-CoV-2
287 pathogenesis, but it has not been determined if the cytokines contribute more to suppressing
288 viral replication, or suppressing the immune response through their anti-inflammatory abilities,
289 contributing to greater disease (50,51). Therefore, it is important to investigate how VOC
290 differentially engage interferon production and subsequently the expression of interferon
291 stimulated genes, during infection. Delta challenge causes a significant increase in lung and
292 serum IFNy which is greater than what has been previously reported in K18-hACE2 mice using
293 different challenge strains such as ancestral WA-1 (30,31,32). IFNy is a potent antiviral cytokine
294 that occurs later in the timeline of viral challenge and may not be observable in widely used
295 COVID-19 mouse models because of short survival lengths (52). IFNy production is typically
296 associated with the activation of Natural Killer cells, innate lymphoid cells, or Th1-like adaptive
297 immune cells (44). Its high concentrations in the lung of Delta mice could corroborate greater
298 recruitment of these cell populations identified in histopathology data as infiltrating cells (Fig. 3).
299 Together the observations of this study suggest that Delta challenge causes enhanced innate
300 immune responses compared to Alpha.

301 Surprisingly we observed that the viral RNA burden of the respiratory tract was identical per day
302 per variant in the K18-hACE2-mice, as determined by both RT-qPCR and RNAseq, a clear
303 question remains: why does Delta induce more interferon responses? One possible option that
304 could be explored is the interaction of viral sgRNAs in regulating host gene expression. Open
305 Reading Frames (ORFs) of SARS-CoV-2 have been implicated in controlling the host anti-viral
306 response (53). Studies have reported that the increase in viral burden due to Alpha leads to
307 increases in some but not all sub-genomic RNAs from the genomic regions harboring variant-

308 characteristic mutations (54). Another study links the expression of sub-genomic RNAs in Alpha
309 infection, specifically ORF9b, to antagonism of the host immune response and suppression of
310 ISGs which would allow for more efficient viral replication and enhanced transmission (55).
311 Although viral gene reads in our analysis show no significant differences between Alpha and
312 Delta sgRNAs, it is possible that our selected timepoints were too late to detect the differences
313 previously reported at 10 and 24 hours post challenge, or that our challenge dose was too low.
314 Still, our abundant transcriptomic data suggest an extensive list of gene pathways that were
315 enriched during Delta but not Alpha infection.

316 We observed that 10^3 PFU challenge with Delta variant does not cause the dramatic weight loss
317 and hypothermia reported in models of Alpha and Beta challenge (17). One well known caveat
318 of the K18-hACE2-mouse model is the fact that WA-1, Alpha and Beta strains enter the brain
319 (43,45,46,56–62). However, it appears that Delta variant remains more localized in the lungs of
320 challenged mice (Fig. 3) (63). It's generally accepted that the K18-hACE2-mice reach morbidity
321 due to brain infection, supported by manifestations of disease including hypothermia, and
322 inflammatory profiles. It is possible that the absence of brain infection due to Delta allows for an
323 increased survival time, leaving more time for the development of severe infection and
324 pneumonia in the lung, which could make Delta a better strain for modeling the respiratory
325 phenotypes of COVID-19 disease in K18-hACE2 mice.

326 We appreciate that the K18-hACE2-mouse model has caveats to consider. The transgenic
327 model expressing human ACE2 in addition to mouse ACE2 addresses SARS-CoV-2's higher
328 affinity for binding human ACE2, which reduces species tropism and allows virus to cause lethal
329 disease in the mice. As is common in transgenic protein expression, hACE2 under the epithelial
330 cell cytokeratin-18 (K18) promoter is not expressed with the identical tissue localization as it
331 would be in humans. Therefore, viral localization should always be carefully considered. Our
332 observations show that Delta accomplishes lung infection in the mouse and induces strong
333 pneumonia. One popular alternative to the K18-hACE2 mouse model is the Syrian Golden

334 Hamster. After SARS-CoV-2 challenge, hamsters develop more observable respiratory disease
335 and pneumonia due to a higher affinity for hamster ACE2 (64,65). Delta has been reported to be
336 highly pathogenic in golden hamsters, with increased tropism for the respiratory tract and low
337 development of disease phenotypes like weight loss and drops in temperature (32,66). The
338 similarities between mouse and hamster models provide evidence for Delta's unique disease
339 manifestation, defending the importance of its use in preclinical models when compared to prior
340 strains.

341 With the emergence of the Omicron variant, it's clear that novel variants of SARS-CoV-2 will
342 continue to arise with enhanced disease capabilities. To continue preclinical COVID-19
343 research with small animal models, strains that more accurately recapitulate present human
344 disease are necessary. Understanding the unique disease mechanisms of each VOC and the
345 caveats they may present in these models will help to advance research into the identification or
346 improvement of therapeutics.

347 The K18-hACE2-mouse challenge model of COVID-19 holds high value in characterizing
348 variants, evaluating vaccines and therapeutics, and defining the pathogenic mechanisms of
349 SARS-CoV-2. The data presented here show that a sublethal challenge with Delta induces
350 inflammation that is more histopathological than the Alpha VOC and increases interferon
351 responses. This study also defines the doses of SARS-CoV-2 VOC that are useful for
352 considering in performing preclinical studies. The use of RNAseq allowed us to characterize the
353 entire transcriptome of the mouse lung to understand the effect of challenge by either Alpha or
354 Delta variants. We observed massive differential gene expression caused by Delta despite that
355 fact that the mice did not reach morbidity. Our study identified unexpected and uncharacteristic
356 aspects of Delta's disease pathogenesis. Together, our study outcomes underscore the need to
357 continue to understand SARS-CoV-2 especially outside of the immunogenicity differences of the
358 spike protein that are most often focused upon. We plan to build upon the findings of this study

359 and characterize single-cell gene expression of the host response in a continued effort seeking
360 to understand ways to combat this virus.

361

362 **Materials and methods**

363 **Biosafety, Animal, and Ethics statement.**

364 All research performed was approved by West Virginia University IACUC protocol number
365 2004034204. K18-hACE2-mice were purchased from Jackson Laboratory (B6.Cg-Tg(K18-
366 ACE2)2PrImln/J; JAX strain number #034860). All SARS-CoV-2 viral propagation or challenge
367 studies were conducted in the West Virginia University Biosafety Laboratory Level 3 facility
368 under the IBC protocol number 20-04-01. SARS-CoV-2 challenged mouse serum and lung
369 supernatant were inactivated with 1% Triton per volume before exiting high containment.
370 Additional tissues were treated using TRIzol reagent or fixed before additional work in BSL2
371 conditions.

372

373 **SARS-CoV-2 cultivation and K18-hACE2 mouse challenge.**

374 SARS-CoV-2 strains were obtained from BEI: USA-WA-1/2020 (WA-1; BEI NR-52281)
375 (GenBank accession number: MN985325), hCoV19/England/204820464/2020 (Alpha; NR-
376 54000)(GISAID: EPI_ISL_683466), and hCoV19/South Africa/KRISP-EC-K005321/2020 (Beta;
377 BEI NR-54008) (GISAID: EPI_ISL_678570). The SARS-CoV-2 Delta variant (B.1.617.2 hCoV-
378 19/USA/WV-WVU-WV118685/2021) was obtained from a patient viral transport medium swab
379 (GISAID Accession ID: EPI_ISL_1742834). SARS-CoV-2 strains were propagated in Vero E6
380 cells (ATCC-CRL-1586). For variant comparison studies, K18-hACE2 mice were intranasally
381 challenged with a volume of 50 uL (25uL per nare) at: 10³ PFU/dose (8 week old male and
382 female received WA-1 or Beta; 12 week old female mice received Alpha; 14 week old female
383 received Delta), or 10⁴ PFU/dose (17 week old female received WA-1; 8 week old male and
384 female received Alpha or Beta; 20 week old female received Delta). Male age-matched mice at

385 8 weeks old were infected with 10³ PFU for timepoint comparison study. Viral doses were
386 prepared from the first passage collections from infected Vero E6 cells. Mice were anesthetized
387 with IP injection of ketamine (Patterson Veterinary 07-803-6637) /xylazine (Patterson Veterinary
388 07-808-1947).

389

390 **Disease score of SARS-CoV-2 challenged mice.**

391 Challenged K18-hACE2 mice were evaluated daily through both in-person health assessments
392 in the BSL3 and SwifTAG Systems video monitoring for out to 14 days post challenge. Health
393 assessments of the mice were scored based on the following criteria: weight loss (scale 0-5 (up
394 to 20% weight loss)), appearance (scale 0-2), activity (scale 0-3), eye closure (scale 0-2), and
395 respiration (scale 0-2). All five criteria were scored based off a scaling system where 0
396 represents no symptoms and the highest number on the scale denotes the most severe
397 phenotype. Additive health scores of the criteria listed above were assigned to each mouse after
398 evaluation. Mice that scored 5 or above on the health assessment required immediate
399 euthanasia. Average cumulative disease scoring was calculated by adding the disease scores
400 of each mouse from the group on each day and reporting the mean. Morbid mice that were
401 euthanized during the study, before day 14, retained their disease score for the remainder of the
402 experiment.

403

404 **Euthanasia and tissue collection.**

405 Mice were euthanized either when assigned a health score of 5 or above or at the end of the
406 experiment with an IP injection of Euthasol (390mg/kg) (Pentobarbital) followed by secondary
407 measure of euthanasia with cardiac puncture. Blood from cardiac puncture was collected in BD
408 Microtainer gold serum separator tubes (Catalog No: 365967), centrifuged at 15,000 x g for 5
409 minutes and serum collected for downstream analysis. Nasal wash was acquired by pushing
410 1mL of PBS through the nasal pharynx. 500µL of nasal wash was added to 500µL of TRI

411 reagent for RNA purification and the remainder of the nasal wash was frozen for serological
412 analysis. Lungs were separated into right and left lobes. Right lobe of the lung was
413 homogenized in 1mL of PBS in gentleMACS C tubes (order number: 130-096-334) using the
414 m_lung_02 program on the gentleMACS Dissociator. 300µL of lung homogenate was added to
415 1000µL of TRI Reagent (Zymo research) for downstream RNA purification and 300 µL of lung
416 homogenate was centrifuged at 15,000 x g for 5 minutes and the lung supernatant was
417 collected for downstream analyses. Brain was excised from the skull and homogenized in 1mL
418 PBS in gentleMACS C tubes using the same setting as lung on the gentleMACS Dissociator.
419 1000µL of TRI Reagent was added to 500µL of brain homogenate for RNA purification.

420

421 **qPCR SARS-CoV-2 viral copy number analysis of lung, brain, and nasal wash.**

422 RNA purification of the lung, brain and nasal wash was performed using the Direct-zol RNA
423 miniprep kit (Zymo Research R2053) following the manufacturer protocol. SARS-CoV-2 copy
424 numbers were assessed through qPCR using the Applied Biosystems TaqMan RNA to CT One
425 Step Kit (Ref: 4392938). We utilized nucleocapsid primers (F: ATGCTGCAATCGTGCTACAA;
426 R: GACTGCCGCCTCTGCTC); and TaqMan probe (IDT:/56-
427 FAM/TCAAGGAAC/ZEN/AACATTGCCAA/3IABkFQ/) that were synthesized according to
428 Winkler. *et al*, 2020 (43). The following final concentrations were used according to the Applied
429 Biosystems TaqMan RNA to CT One Step Kit manufacturer protocol: TaqMan RT-PCR Mix 2X,
430 Forward and reverse primers 900nM final, TaqMan probe 250nM final, TaqMan RT enzyme mix
431 40X and RNA template 100ng (excluding Nasal Wash). Purified RNA samples with a
432 concentration less than 100ng/uL were not diluted for use in qPCR reactions. All Nasal Wash
433 RNA samples were used at a set volume of 2 uL due to low RNA quantification via the Qubit 3
434 fluorometer. Triplicates were prepared for each sample, and samples were loaded into a
435 MicroAmp Fast optical 96 well reaction plate (Applied Biosystems 4306737). Prepared reactions
436 were run on the StepOnePlus Real-Time System machine using the parameters: Reverse

437 transcription for 15 minutes at 48°C, activation of AmpliTaq Gold DNA polymerase for 10
438 minutes at 95°C, and 50 cycles of denaturing for 15 seconds at 95°C and annealing at 60°C for
439 1 minute.

440

441 **Cytokine analysis**

442 R&D 5-plex mouse magnetic Luminex assay (Ref LXSAMSM) was used to quantify cytokines:
443 IL-1 β , CXCL13, TNF α , IL-6, IFN- γ , IL-17, and CXCL10 from lung supernatant. Manufacturer
444 protocols were followed in preparing samples. Mouse cytokine plate was analyzed on the
445 Luminex Magpix and pg/mL were calculated based off standard curves generated for each
446 cytokine in the assay. IFN- α , IFN- β and IFN- γ were additionally quantified using MSD U-PLEX
447 Interferon Combo 1 (ms) assay kit (Catalog No K15320K-1) and manufacturer protocols. MSD
448 assay plates were analyzed using the Meso Scale Discovery Sector 2400.

449

450 **Histology and Electron microscopy**

451 Left lobes of lungs were immediately fixed in 10mL of 10% neutral buffered formalin. Fixed
452 lungs were paraffin embedded into 5 μ m sections. Sections were stained with hematoxylin and
453 eosin and visualized on the DynamyxTM digital pathology platform. Lungs were scored for
454 chronic and acute inflammation in the lung parenchyma, blood vessels, and airways by a
455 blinded pathologist. Pulmonary inflammation was quantified by measuring the total area of lung
456 tissue involved by inflammation. The predominant inflammatory cell type was noted. To quantify
457 vascular margination of inflammatory cells, five representative arteries were identified within
458 areas involved by inflammation. Total length of endothelium of these vessels was measured and
459 the number of marginating inflammatory cells in the cross section were manually counted.
460 Areas involved by inflammation were further evaluated by electron microscopic examination.
461 The areas of interest were punched from the paraffin embedded tissue block and processed for
462 electron microscopy. Ultrathin sections were cut on a Leica Ultra-Microtome, collected on

463 copper mesh grids, stained using uranyl acetate and lead citrate and viewed using a Jeol 1010
464 electron microscope (FEI) with attached AMT camera.

465

466 **Illumina library preparation, sequencing, and *in silico* bioinformatic analysis**

467 RNA quantity was measured with Qubit 3.0 Fluorometer using the RNA high sensitivity (Life
468 Technologies) and RNA integrity was assessed using an Agilent TapeStation. RNA was
469 DNaseased before library preparation. Illumina sequencing libraries were prepared with KAPA
470 RNA HyperPrep Kit with RiboErase (Basel, Switzerland). Resulting libraries passed standard
471 Illumina quality control PCR and were sequenced on an Illumina NovaSeq s4 4000 at Admera
472 Health (South Plainfield, NJ). A total of ~100 million 150 base pair reads were acquired per
473 sample. Sequencing data will be deposited to the Sequence Read Archive. The reads were
474 trimmed for quality and mapped to the *Mus musculus* reference genome using CLC Genomics
475 Version 21.0.5. Two mice were excluded due to no detectable viral reads (n=5 NC, 4 Alpha
476 Day 2, 5 Alpha Day 6, 5 Delta Day 2, 4 Delta Day 6). An exported gene expression browser
477 table is available upon request. Statistical analysis was performed with the Differential
478 Expression for RNA Seq tool and genes were annotated with the reference mouse gene
479 ontology terms. Quantification of the number of activated or repressed genes unique to each
480 experimental group was performed using Venny 2.1 (67). Genes from each experimental
481 comparison with significant fold changes (Bonferroni ≤ 0.04) were submitted to the WEB-based
482 Gene SeT AnaLysis Toolkit's Over Representation Analysis (ORA) software compared to the
483 reference set "affy mg u74a" to determine GO terms from gene ontology and biological process
484 databases (FDR ≤ 0.05) (68). GO Term heat maps were generated using Morpheus (69). Raw
485 read data is available at NCBI SRA: SUB10957945 (submission complete, pending processing).

486

487 **Statistical analyses**

488 All statistical analyses were performed using GraphPad Prism version 9. Statistical analyses
489 were performed with $n \geq 3$ for all K18-ACE2 mice studies. Ordinary one-way ANOVA with
490 Dunnett's multiple comparisons test or Two-Way ANOVA with Tukey's multiple comparisons
491 test were used with single pooled variance for data sets following a normal distribution and
492 Kruskal-Wallis with Dunn's multiple comparisons test for non-parametric distributed datasets.
493 Kaplan-Meier survival curves were utilized, and Log-rank (Mantel-Cox) test were used to test
494 significance of survival between sample groups.

495

496 **Acknowledgements**

497 This project was supported by the Vaccine Development Center at the West Virginia University
498 Health Sciences Center. F.H.D. and the VDC are supported by the Research Challenge Grant
499 no. HEPC.dsr.18.6 from the Division of Science and Research, WV Higher Education Policy
500 Commission. MSD QuickPlex SQ120 in the WVU Flow Cytometry & Single Cell Core Facility is
501 supported by the Institutional Development Awards (IDeA) from the National Institute of General
502 Medical Sciences of the National Institutes of Health under grant numbers P30GM121322 (TME
503 CoBRE) and P20GM103434 (INBRE). Figure preparation was supported by GraphPad Prism
504 and BioRender.

505 We would like to acknowledge Mary Tomago-Chesney for sectioning and performing H&E
506 staining on tissues. We would like to thank the Electron Microscopy, Histopathology and Tissue
507 Bank Core for obtaining Electron Microscopy images of the delta variant in lungs. Lastly, we
508 thank Drs. Laura Gibson and Clay Marsh for supporting this COVID-19 vaccine research.

509

510 **Author contributions.** Studies were designed by FHD, KSL, JRB, AMH. All authors contributed
511 to the execution of the studies. MTW and IM prepared and provided titered viral stocks of WA-1,
512 Alpha, Beta, and Delta SARS-CoV-2 for challenge. Animal health checks, necropsy, and tissue
513 processing were performed by FHD, TYW, BRP, KSL, JRB, OAM, AMH, and HAC. Viral RNA

514 qPCR was performed by HAC and OAM. Serological analysis was executed by KSL, and NAR.
515 Luminex cytokine assays were completed by BPR. MSD assays were performed by KSL. Lung
516 tissue samples were histologically scored by MSA and JPG. Data was analyzed by KSL, AMH,
517 and FHD. All authors contributed to the writing and revision of this manuscript.

518

519 **Conflicts of interest.** none

520

521 **Figures and Legends**

522 **Figure 1. Survival, disease scores, weight, and temperature of K19-hACE2-mice**
523 **challenged with WA-1, Alpha, Beta, and Delta strains.** K18-hACE2 transgenic mice were
524 intranasally challenged with 1×10^3 or 1×10^4 PFU WA-1, Alpha (B.1.1.7), Beta (B.1.351) or Delta
525 (B.1.617) SARS-CoV-2, or mock-challenged with PBS (NC). Post-challenge, mouse survival (A,
526 B) (n=4 for 1×10^3 WA-1, n=7 for 1×10^4 WA-1, n=3 for 1×10^3 Alpha, n=4 for 1×10^4 Alpha, n=4 for
527 1×10^3 Beta, n=4 for 1×10^4 Beta, n=5 for 1×10^3 Delta and n=10 for 1×10^4 Delta) and disease
528 scores (C, D) were evaluated. Based on experimental results, mice challenged with Alpha (n=10
529 split between timepoints) and Delta (n=10 split between timepoints) or mock-challenged with
530 PBS (n=5), were evaluated at day 2 and day 6 post-challenge to measure changes in
531 bodyweight (E, F) and body rectal temperature (G, H). Dotted lines indicate euthanasia points
532 on day 2, day 5 (euthanasia of mock-challenge controls) and day 6. NC=no challenge.

533 **Figure 2. Viral RNA burden of disease-associated tissues was quantified using**
534 **nucleocapsid qPCR.** Viral RNA was detectable in the lung tissue of challenged mice from both
535 variants at both timepoints compared to no challenge (One-Way ANOVA, $P=0.0008$; 0.0004 ;
536 0.0003 ; 0.0013) (A). In Nasal Wash, viral RNA burden increased from both variants at Day 2
537 compared to no challenge (One-Way ANOVA, $P=0.0016$ Alpha; $P=0.0030$ Delta) and was
538 decreased at Day 6 for both variants from copy numbers at Day 2 (One-Way ANOVA, $P=0.0043$

539 Alpha; $P=0.0019$ Delta) (B). Alpha challenged mice have increased detectable viral RNA in the
540 brain at Day 6 compared to Day 2 (One-Way ANOVA, $P=0.0012$) while Delta challenge results
541 in no viral RNA burden in the brain (C). Dashed lines indicate limit of detection via qPCR.
542 NC=no challenge.

543 **Figure 3. Histopathological and electron microscopy analysis of Alpha or Delta**
544 **challenged K18-hACE2-mouse lungs.** 20X images demonstrating inflammation in the lung
545 tissue of Alpha and Delta SARS-CoV-2 challenged K18-hACE2 at Day 2 or 6 post-challenge (B)
546 compared to no challenge (A). 20X images reveal margination at blood vessels within areas of
547 inflammation (green arrows indicate counted marginating cells, red arrows indicate tissue-
548 resident non-marginating cells)(C). Marginating inflammatory cells were counted within the
549 tissue and were found to be increased in Delta challenge at Day 6 (Kruskal Wallis One-Way
550 ANOVA, $P=0.0097$) (D). Regional tissue inflammation was quantified as % total area of
551 analyzed tissue (mm^3) and was highest in Delta at Day 6 compared to no challenge (Kruskal
552 Wallis One-Way ANOVA, $P=0.0012$) (E). Error bars represent SD. Electron microscopy images
553 displayed distribution of Delta virus particles in 1×10^3 PFU challenged mouse lung tissue (F,G).
554 White arrows identify virions.

555 **Figure 4. Analysis of cytokines production in lung supernatants from Alpha or Delta**
556 **challenged K18-hACE2 transgenic mice at 2 or 6 days post-challenge.** Non-challenged,
557 Alpha or Delta challenged lung supernatants were used to determine local cytokine production
558 in response to challenge. Concentrations (pg/mL) were graphed using Morpheus to reveal
559 relative levels of cytokines compared to non-challenged lungs.

560 **Figure 5. RNAseq analysis of SARS-CoV-2 genes in challenged mouse lungs.** Schematic
561 of the SARS-CoV-2 genome (A). Total viral read counts in each group (B) as well as
562 quantification of viral reads per 1M RNAseq reads obtained (C). Reads of human ACE2 gene of
563 the K18-hACE2-mice were quantified per 50M reads obtained per lung sample (D).

564 **Figure 6. Total transcriptomic analysis of mouse genes in non-challenged mice**
565 **compared to Alpha and Delta challenged mice at days 2 and 6.** RNAseq reads from
566 challenged mice were compared to non-challenged mice to determine differential gene
567 expression (A). Genes that were statistically significant are indicated in relation to challenge
568 day and their relative expression as being activated or repressed. Venn diagrams are shown to
569 illustrate the amount of overlap in significant genes between days 2 and 6. The total number of
570 unique differentially expressed genes are represented per each challenge day and relative
571 expression (B). The highest differentially activated genes are show per each group with fold
572 change relative to non-challenged control RNAseq reads (C). Gene expression of activated
573 genes are ranked by fold change in Delta day 6 mice and then shown in relation to both strains
574 and days post challenge (D).

575 **Figure 7 Gene ontology analysis of systems of genes in challenged mice.** Circle plots
576 indicate the number of unique or conserved sets of genes that were found to be enriched per
577 each group (A). The top 30 enriched GO terms are shown and plotted per their relative level of
578 expression and enrichment ratio (B). TCR clonotypes were mapped and represented as Total
579 clones (C) or unique clones per unique CDR3 sequence (D). Total TCR clones ($P=0.0005$) and
580 unique clones were increased between Delta day 2 and day 6 ($P<0.0001$).

581 **Figure 8 Analysis of interferon dependent gene expression and production of type I and**
582 **type II interferon in lungs and serum of K18-hACE2-mice.** Total RNA counts per interferon
583 dependent gene are shown per each mouse, time-point, and variant challenge group (A). Each
584 square represents the total RNA counts per gene from one mouse. Interferon dependent genes
585 are shown with relative fold change plotted (B). Interferon alpha, beta, and gamma production
586 in lung supernatant (C) and serum (D) of K18-hACE2-mice.

587

588 **References**

589 1. Galloway SE, Paul P, Maccannell DR, Johansson MA, Brooks JT, Macneil A, et al.

590 Emergence of SARS-CoV-2 B.1.1.7 Lineage — United States, December 29, 2020–
591 January 12, 2021 [Internet]. 2021 [cited 2022 Jan 4]. Available from:
592 <https://www.cdc.gov/coronavirus/2019-ncov/more/science-and-research/>

593 2. Tegally H, Wilkinson E, Giovanetti M, Iranzadeh A, Fonseca V, Giandhari J, et al.
594 Detection of a SARS-CoV-2 variant of concern in South Africa. *Nature*. 2021 Apr
595 15;592(7854):438–43.

596 3. da Silva JC, Félix VB, Leão SABF, Trindade-Filho EM, Scorza FA. New Brazilian variant
597 of the SARS-CoV-2 (P1/Gamma) of COVID-19 in Alagoas state. *Braz J Infect Dis*
598 [Internet]. 2021 May 1 [cited 2022 Jan 12];25(3). Available from:
599 <https://pubmed.ncbi.nlm.nih.gov/34102147/>

600 4. Faria N, Et-al. Genomic characterisation of an emergent SARS-CoV-2 lineage in Manaus:
601 preliminary findings - SARS-CoV-2 coronavirus / nCoV-2019 Genomic Epidemiology -
602 Virological [Internet]. *virological.org*. 2021 [cited 2022 Jan 12]. Available from:
603 [https://virological.org/t/genomic-characterisation-of-an-emergent-sars-cov-2-lineage-in-
604 manaus-preliminary-findings/586](https://virological.org/t/genomic-characterisation-of-an-emergent-sars-cov-2-lineage-in-manaus-preliminary-findings/586)

605 5. Hitchings MDT, Ranzani OT, Dorion M, D'Agostini TL, de Paula RC, de Paula OFP, et al.
606 Effectiveness of ChAdOx1 vaccine in older adults during SARS-CoV-2 Gamma variant
607 circulation in São Paulo. *Nat Commun* [Internet]. 2021 [cited 2022 Jan 12];12(1).
608 Available from: <https://doi.org/10.1038/s41467-021-26459-6>

609 6. Charmet T, Schaeffer L, Grant R, Galmiche S, Chény O, Von Platen C, et al. Impact of
610 original, B.1.1.7, and B.1.351/P.1 SARS-CoV-2 lineages on vaccine effectiveness of two
611 doses of COVID-19 mRNA vaccines: Results from a nationwide case-control study in
612 France. *Lancet Reg Heal - Eur*. 2021 Sep;8:100171.

613 7. Hall VJ, Foulkes S, Saei A, Andrews N, Oguti B, Charlett A, et al. COVID-19 vaccine
614 coverage in health-care workers in England and effectiveness of BNT162b2 mRNA
615 vaccine against infection (SIREN): a prospective, multicentre, cohort study. *Lancet*. 2021

616 May 8;397(10286):1725–35.

617 8. Shinde V, Bhikha S, Hoosain Z, Archary M, Bhorat Q, Fairlie L, et al. Efficacy of NVX-
618 CoV2373 Covid-19 Vaccine against the B.1.351 Variant. *N Engl J Med.* 2021 May
619 20;384(20):1899–909.

620 9. Madhi SA, Baillie V, Cutland CL, Voysey M, Koen AL, Fairlie L, et al. Efficacy of the
621 ChAdOx1 nCoV-19 Covid-19 Vaccine against the B.1.351 Variant. *N Engl J Med.* 2021
622 May 20;384(20):1885–98.

623 10. Sadoff J, Gray G, Vandebosch A, Cárdenas V, Shukarev G, Grinsztejn B, et al. Safety
624 and Efficacy of Single-Dose Ad26.COV2.S Vaccine against Covid-19. *N Engl J Med.*
625 2021;384(23):2187–201.

626 11. Grabowski F, Preibisch G, Giziński S, Kochańczyk M, Lipniacki T. Sars-cov-2 variant of
627 concern 202012/01 has about twofold replicative advantage and acquires concerning
628 mutations. *Viruses* [Internet]. 2021 Mar 1 [cited 2022 Jan 12];13(3). Available from:
629 <https://pubmed.ncbi.nlm.nih.gov/33804556/>

630 12. Grint DJ, Grint DJ, Wing K, Houlihan C, Gibbs HP, Evans SJW, et al. Severity of Severe
631 Acute Respiratory System Coronavirus 2 (SARS-CoV-2) Alpha Variant (B.1.1.7) in
632 England. *Clin Infect Dis* [Internet]. 2021 Sep 6 [cited 2022 Jan 12]; Available from:
633 <https://academic.oup.com/cid/advance-article/doi/10.1093/cid/ciab754/6365124>

634 13. Lin L, Liu Y, Tang X, He D. The Disease Severity and Clinical Outcomes of the SARS-
635 CoV-2 Variants of Concern. *Front Public Heal.* 2021 Nov 30;9:1929.

636 14. Patone M, Thomas K, Hatch R, Tan PS, Coupland C, Liao W, et al. Mortality and critical
637 care unit admission associated with the SARS-CoV-2 lineage B.1.1.7 in England: an
638 observational cohort study. *Lancet Infect Dis.* 2021 Nov 1;21(11):1518–28.

639 15. Davies NG, Abbott S, Barnard RC, Jarvis CI, Kucharski AJ, Munday JD, et al. Estimated
640 transmissibility and impact of SARS-CoV-2 lineage B.1.1.7 in England. *Science* (80-)
641 [Internet]. 2021 Apr 9;372(6538). Available from:

642 https://www.science.org/doi/10.1126/science.abg3055

643 16. Veneti L, Seppälä E, Storm ML, Salamanca BV, Buanes EA, Aasand N, et al. Increased
644 risk of hospitalisation and intensive care admission associated with reported cases of
645 SARS-CoV-2 variants B.1.1.7 and B.1.351 in Norway, December 2020–May 2021. Vol.
646 16, PLoS ONE. Public Library of Science; 2021.

647 17. Radvak P, Kwon HJ, Kosikova M, Ortega-Rodriguez U, Xiang R, Phue JN, et al. SARS-
648 CoV-2 B.1.1.7 (alpha) and B.1.351 (beta) variants induce pathogenic patterns in K18-
649 hACE2 transgenic mice distinct from early strains. *Nat Commun.* 2021 Dec 1;12(1).

650 18. Bayarri-Olmos R, Bruun Johnsen L, Idorn M, Reinert LS, Rosbjerg A, Vang S, et al. The
651 alpha/B.1.1.7 SARS-CoV-2 variant exhibits significantly higher affinity for ACE-2 and
652 requires lower inoculation doses to cause disease in K18-hACE2 mice. *eLife* [Internet].
653 2021 [cited 2022 Jan 5]; Available from: <https://doi.org/10.7554/eLife.70002>

654 19. Tregoning JS, Flight KE, Higham SL, Wang Z, Pierce BF. Progress of the COVID-19
655 vaccine effort: viruses, vaccines and variants versus efficacy, effectiveness and escape.
656 Vol. 21, *Nature Reviews Immunology*. Nature Research; 2021. p. 626–36.

657 20. Lopez Bernal J, Andrews N, Gower C, Gallagher E, Simmons R, Thelwall S, et al.
658 Effectiveness of Covid-19 Vaccines against the B.1.617.2 (Delta) Variant. *N Engl J Med.*
659 2021 Aug 12;385(7):585–94.

660 21. Singh J, Rahman SA, Ehtesham NZ, Hira S, Hasnain SE. SARS-CoV-2 variants of
661 concern are emerging in India. Vol. 27, *Nature Medicine*. Nature Research; 2021. p.
662 1131–3.

663 22. Nasreen S, He Msc S, Mph HC, Brown Phd KA, Gubbay JB, Buchan SA, et al.
664 Effectiveness of COVID-19 vaccines against variants of concern, Canada on behalf of the
665 Canadian Immunization Research Network (CIRN) Provincial Collaborative Network
666 (PCN) Investigators. *medRxiv* [Internet]. 2021;2021.06.28.21259420. Available from:
667 <https://doi.org/10.1101/2021.06.28.21259420>

668 23. Christensen PA, Olsen RJ, Wesley Long S, Subedi S, Davis J, Hodjat P, et al. Delta
669 variants of SARS-CoV-2 cause significantly increased. medRxiv [Internet]. 2021 Oct 7;
670 Available from: <https://doi.org/10.1101/2021.07.19.21260808>

671 24. Dagan N, Barda N, Kepten E, Miron O, Perchik S, Katz MA, et al. BNT162b2 mRNA
672 Covid-19 Vaccine in a Nationwide Mass Vaccination Setting. *N Engl J Med.* 2021 Apr
673 15;384(15):1412–23.

674 25. Deng X, Garcia-Knight MA, Khalid MM, Servellita V, Wang C, Morris MK, et al.
675 Transmission, infectivity, and neutralization of a spike L452R SARS-CoV-2 variant. *Cell*
676 [Internet]. 2021 Jun 24 [cited 2022 Jan 12];184(13):3426-3437.e8. Available from:
677 <http://www.cell.com/article/S0092867421005055/fulltext>

678 26. Greaney AJ, Loes AN, Crawford KHD, Starr TN, Malone KD, Chu HY, et al.
679 Comprehensive mapping of mutations in the SARS-CoV-2 receptor-binding domain that
680 affect recognition by polyclonal human plasma antibodies. *Cell Host Microbe* [Internet].
681 2021 Mar 10 [cited 2022 Jan 12];29(3):463-476.e6. Available from:
682 <http://www.cell.com/article/S1931312821000822/fulltext>

683 27. Planas D, Veyer D, Baidaliuk A, Staropoli I, Guivel-Benhassine F, Rajah MM, et al.
684 Reduced sensitivity of SARS-CoV-2 variant Delta to antibody neutralization. *Nature.* 2021
685 Aug 12;596(7871):276–80.

686 28. Liu Y, Liu J, Plante KS, Plante JA, Xie X, Zhang X, et al. The N501Y spike substitution
687 enhances SARS-CoV-2 transmission. *bioRxiv* [Internet]. 2021 Mar 9; Available from:
688 <https://doi.org/10.1101/2021.03.08.434499>

689 29. Plante JA, Liu Y, Liu J, Xia H, Johnson BA, Lokugamage KG, et al. Spike mutation
690 D614G alters SARS-CoV-2 fitness. *Nature.* 2021 Apr 1;592(7852):116–21.

691 30. Arora P, Kempf A, Nehlmeier I, Graichen L, Sidarovich A, Winkler MS, et al. Delta variant
692 (B.1.617.2) sublineages do not show increased neutralization resistance [Internet]. Vol.
693 18, *Cellular and Molecular Immunology*. Nature Publishing Group; 2021 [cited 2022 Jan

694 12]. p. 2557–9. Available from: <https://www.nature.com/articles/s41423-021-00772-y>

695 31. Kannan SR, Spratt AN, Cohen AR, Naqvi SH, Chand HS, Quinn TP, et al. Evolutionary
696 analysis of the Delta and Delta Plus variants of the SARS-CoV-2 viruses. *J Autoimmun*
697 [Internet]. 2021 Nov 1 [cited 2022 Jan 12];124:102715. Available from:
698 [/pmc/articles/PMC8354793/](https://www.ncbi.nlm.nih.gov/pmc/articles/PMC8354793/)

699 32. Saito A, Irie T, Suzuki R, Maemura T, Nasser H, Uriu K, et al. Enhanced fusogenicity and
700 pathogenicity of SARS-CoV-2 Delta P681R mutation. *Nature* [Internet]. 2021; Available
701 from: <https://doi.org/10.1038/s41586-021-04266-9>

702 33. Makdasi E, Zvi A, Alcalay R, Noy-Porat T, Peretz E, Mechaly A, et al. The neutralization
703 potency of anti-SARS-CoV-2 therapeutic human monoclonal antibodies is retained
704 against viral variants. *Cell Rep*. 2021 Sep 7;36(10).

705 34. Hunt AC, Case JB, Park Y-J, Cao L, Wu K, Walls AC, et al. Multivalent designed proteins
706 protect against SARS-CoV-2 variants of concern. *bioRxiv Prepr Serv Biol* [Internet]. 2021
707 Jul 7; Available from: <http://www.ncbi.nlm.nih.gov/pubmed/34268509>

708 35. Stone S, Rothan HA, Natekar JP, Kumari P, Sharma S, Pathak H, et al. SARS-CoV-2
709 variants of concern infect the respiratory tract and induce inflammatory response in wild-
710 type laboratory mice [Internet]. 2021. Available from:
711 <https://doi.org/10.1101/2021.09.29.462373>

712 36. Shuai H, Chan JFW, Yuen TTT, Yoon C, Hu JC, Wen L, et al. Emerging SARS-CoV-2
713 variants expand species tropism to murines. *EBioMedicine*. 2021 Nov 1;73.

714 37. Thakur N, Gallo G, Newman J, Peacock TP, Biasetti L, Hall CN, et al. SARS-CoV-2
715 variants of concern Alpha, Beta, Gamma and Delta have extended ACE2 receptor host-
716 ranges. *bioRxiv* [Internet]. 2021; Available from:
717 <https://doi.org/10.1101/2021.11.23.469663>

718 38. Kant R, Kareinen L, Smura T, Freitag TL, Jha SK, Alitalo K, et al. Common laboratory
719 mice are susceptible to infection with the SARS-CoV-2 beta variant. *Viruses*. 2021 Nov

720 1;13(11).

721 39. Montagutelli X, Prot M, Levillayer L, Salazar EB, Jouvion G, Conquet L, et al. The B1.351
722 and P.1 variants extend SARS-CoV-2 host range to mice. *bioRxiv* [Internet]. 2021 Mar 18
723 [cited 2022 Jan 9];2021.03.18.436013. Available from:
724 <https://www.biorxiv.org/content/10.1101/2021.03.18.436013v1>

725 40. Moreau GB, Burgess SL, Sturek JM, Donlan AN, Petri WA, Mann BJ. Evaluation of K18-
726 hACE2 Mice as a Model of SARS-CoV-2 Infection. *Am J Trop Med Hyg*.
727 2020;103(3):1215–9.

728 41. Muñoz-Fontela C, Dowling WE, Funnell SGP, Gsell P-S, Riveros-Balta AX, Albrecht RA,
729 et al. Animal models for COVID-19. *Nat* 2020 5867830 [Internet]. 2020 Sep 23 [cited
730 2021 Jul 31];586(7830):509–15. Available from: <https://www.nature.com/articles/s41586-020-2787-6>

732 42. Yinda CK, Port JR, Bushmaker T, Owusu IO, Purushotham JN, Avanzato VA, et al. K18-
733 hACE2 mice develop respiratory disease resembling severe COVID-19. *PLoS Pathog*.
734 2021;17(1):1–21.

735 43. Winkler ES, Bailey AL, Kafai NM, Nair S, McCune BT, Yu J, et al. SARS-CoV-2 infection
736 of human ACE2-transgenic mice causes severe lung inflammation and impaired function.
737 *Nat Immunol*. 2020 Nov 1;21(11):1327–35.

738 44. Oladunni FS, Park JG, Pino PA, Gonzalez O, Akhter A, Allué-Guardia A, et al. Lethality of
739 SARS-CoV-2 infection in K18 human angiotensin-converting enzyme 2 transgenic mice.
740 *Nat Commun*. 2020 Dec 1;11(1).

741 45. Yinda CK, Port JR, Bushmaker T, Owusu IO, Purushotham JN, Avanzato VA, et al. K18-
742 hACE2 mice develop respiratory disease resembling severe COVID-19. *PLoS Pathog*.
743 2021 Jan 19;17(1).

744 46. Dong W, Mead H, Tian L, Park J-G, Garcia JI, Jaramillo S, et al. The K18-hACE2
745 Transgenic Mouse Model Recapitulates Non-Severe and Severe COVID-1 19 in

746 Response to Infectious Dose of SARS-CoV-2 Virus 2 3. 2021 [cited 2022 Jan 11];
747 Available from: <https://www.worldometers.info/coronavirus/>

748 47. Ragab D, Salah Eldin H, Taeimah M, Khattab R, Salem R. The COVID-19 Cytokine
749 Storm; What We Know So Far. Vol. 11, *Frontiers in Immunology*. Frontiers Media S.A.;
750 2020.

751 48. Klouda T, Hao Y, Kim H, Kim J, Olejnik J, Hume AJ, et al. Interferon-alpha or -beta
752 facilitates SARS-CoV-2 pulmonary vascular infection by inducing ACE2. *Angiogenesis*.
753 2021;

754 49. Ziegler CGK, Allon SJ, Nyquist SK, Mbano IM, Miao VN, Tzouanas CN, et al. SARS-CoV-
755 2 Receptor ACE2 Is an Interferon-Stimulated Gene in Human Airway Epithelial Cells and
756 Is Detected in Specific Cell Subsets across Tissues. *Cell*. 2020 May 28;181(5):1016-
757 1035.e19.

758 50. McKechnie JL, Blish CA. The Innate Immune System: Fighting on the Front Lines or
759 Fanning the Flames of COVID-19? Vol. 27, *Cell Host and Microbe*. Cell Press; 2020. p.
760 863–9.

761 51. Israelow B, Song E, Mao T, Lu P, Meir A, Liu F, et al. Mouse model of SARS-CoV-2
762 reveals inflammatory role of type I interferon signaling. *J Exp Med*. 2020 Aug 4;217(12).

763 52. Lee AJ, Ashkar AA. The dual nature of type I and type II interferons. *Front Immunol*. 2018
764 Sep 11;9(SEP):2061.

765 53. Zhang Y, Chen Y, Li Y, Huang F, Luo B, Yuan Y, et al. The ORF8 protein of SARS-CoV-2
766 mediates immune evasion through down-regulating MHC-I. *Proc Natl Acad Sci U S A*
767 [Internet]. 2021;118(23). Available from: <https://doi.org/10.1073/pnas.2024202118>

768 54. Matthew Parker AD, Lindsey BB, Shah DR, Hsu S, Biomedical S. Title Altered
769 Subgenomic RNA Expression in SARS-CoV-2 B.1.1.7 Infections Genomics UK (COG-
770 UK) consortium 11+, Thushan I. de Silva 4,5 * Full list of consortium names and

771 affiliations located in the supplementary material *Corresponding Author Affiliations 1.

772 Cariad Evans 4 [Internet]. Available from: <https://doi.org/10.1101/2021.03.02.433156>

773 55. Thorne LG, Bouhaddou M, Reuschl A-K, Zuliani-Alvarez L, Polacco B, Pelin A, et al.

774 Evolution of enhanced innate immune evasion by the SARS-CoV-2 B.1.1.7 UK variant.

775 bioRxiv Prepr Serv Biol [Internet]. 2021 Jun 7; Available from:

776 <http://www.ncbi.nlm.nih.gov/pubmed/34127972>

777 56. McCray PB, Pewe L, Wohlford-Lenane C, Hickey M, Manzel L, Shi L, et al. Lethal

778 Infection of K18- hACE2 Mice Infected with Severe Acute Respiratory Syndrome

779 Coronavirus . J Virol. 2007 Jan 15;81(2):813–21.

780 57. Carosino M, Montanaro P, O'Connell A, Kenney D, Gertje H, Grosz KA, et al. Fatal

781 neuroinvasion of SARS-CoV-2 in K18-hACE2 mice is partially dependent on hACE2

782 expression. bioRxiv Prepr Serv Biol [Internet]. 2021 Jan 15; Available from:

783 <http://www.ncbi.nlm.nih.gov/pubmed/33469581>

784 58. Fumagalli V, Ravà M, Marotta D, Di Lucia P, Laura C, Sala E, et al. Controlled

785 administration of aerosolized SARS-CoV-2 to K18-hACE2 transgenic mice uncouples

786 respiratory infection and anosmia from fatal neuroinvasion 5. Available from:

787 <https://doi.org/10.1101/2021.08.06.455382>

788 59. Kumari P, Rothan HA, Natekar JP, Stone S, Pathak H, Strate PG, et al. Neuroinvasion

789 and Encephalitis Following Intranasal Inoculation of SARS-CoV-2 in K18-hACE2 Mice.

790 2021; Available from: <https://doi.org/10.3390/v13010132>

791 60. Marc A, Kerioui M, Blanquart F, Bertrand J, Mitjà O, Corbacho-Monné M, et al.

792 Quantifying the relationship between sars-cov-2 viral load and infectiousness. Elife. 2021

793 Sep 1;10.

794 61. Chia PY, Ong SWX, Chiew CJ, Ang LW, Chavatte J-M, Mak T-M, et al. Virological and

795 serological kinetics of SARS-CoV-2 Delta variant vaccine-breakthrough infections a multi-

796 center cohort study. Clin Microbiol Infect [Internet]. 2021; Available from:

797 <https://doi.org/10.1016/j.cmi.2021.11.010>

798 62. Kissler SM, Fauver JR, Mack C, Olesen SW, Tai C, Shiue KY, et al. Viral dynamics of
799 acute SARS-CoV-2 infection and applications to diagnostic and public health strategies.
800 PLoS Biol. 2021 Jul 1;19(7).

801 63. Reardon S. How the Delta variant achieves its ultrafast spread. Nature. 2021 Jul 21;

802 64. Sia SF, Yan LM, Chin AWH, Fung K, Choy KT, Wong AYL, et al. Pathogenesis and
803 transmission of SARS-CoV-2 in golden hamsters. Nature. 2020 Jul 30;583(7818):834–8.

804 65. Imai M, Iwatsuki-Horimoto K, Hatta M, Loeber S, Halfmann PJ, Nakajima N, et al. Syrian
805 hamsters as a small animal model for SARS-CoV-2 infection and countermeasure
806 development. PNAS [Internet]. 2020 Jul 14;117(28):16587–95. Available from:
807 www.pnas.org/cgi/doi/10.1073/pnas.2009799117

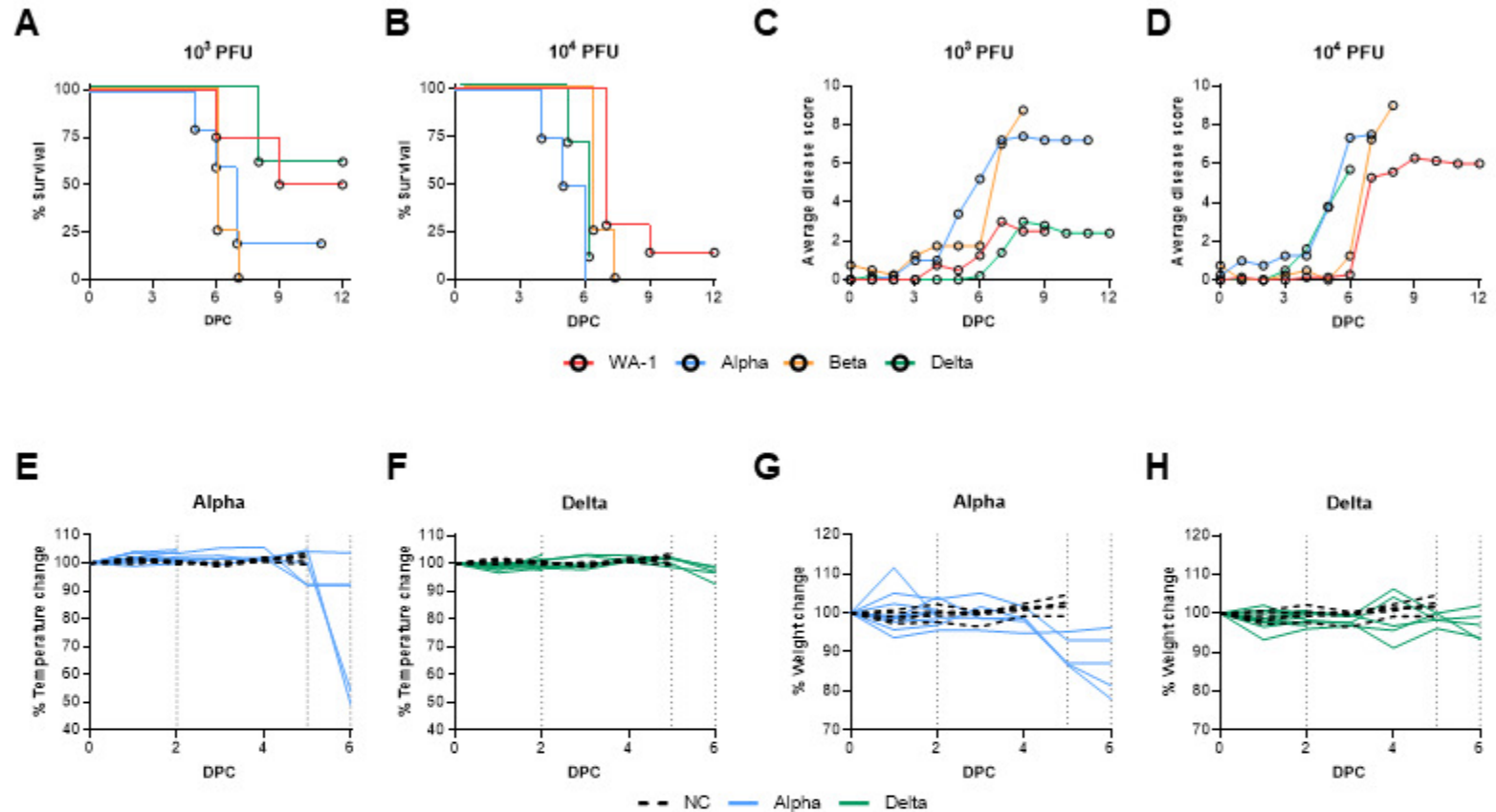
808 66. Mohandas S, Yadav PD, Shete A, Nyayanit D, Sapkal G, Lole K, et al. Sars-cov-2 delta
809 variant pathogenesis and host response in syrian hamsters. Viruses. 2021 Sep 1;13(9).

810 67. Olivers JC. Venny. An interactive tool for comparing lists with Venn’s diagrams [Internet].
811 Available from: <http://bioinfogp.cnb.csic.es/tools/venny/index.html>

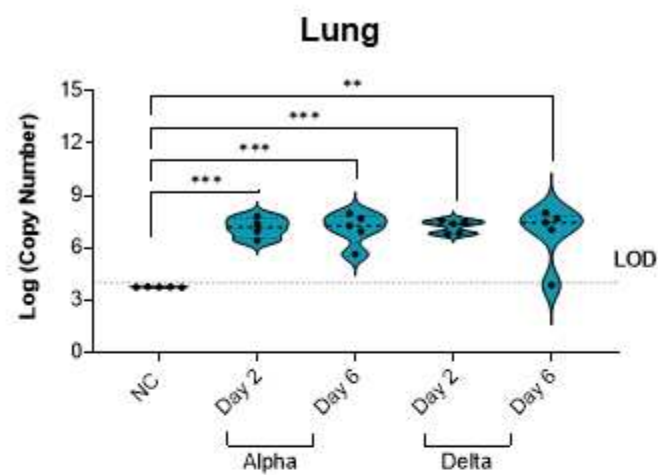
812 68. Liao Y, Wang J, Jaehnig EJ, Shi Z, Zhang B. WebGestalt 2019: gene set analysis toolkit
813 with revamped UIs and APIs. Nucleic Acids Res [Internet]. 2019;47(W1):W199–205.
814 Available from: <http://www.webgestalt.org>.

815 69. Morpheus [Internet]. [cited 2021 Oct 12]. Available from:
816 <https://software.broadinstitute.org/morpheus/>

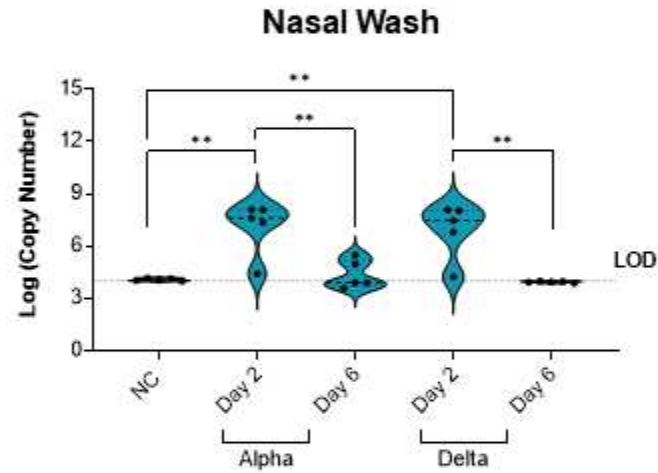
817



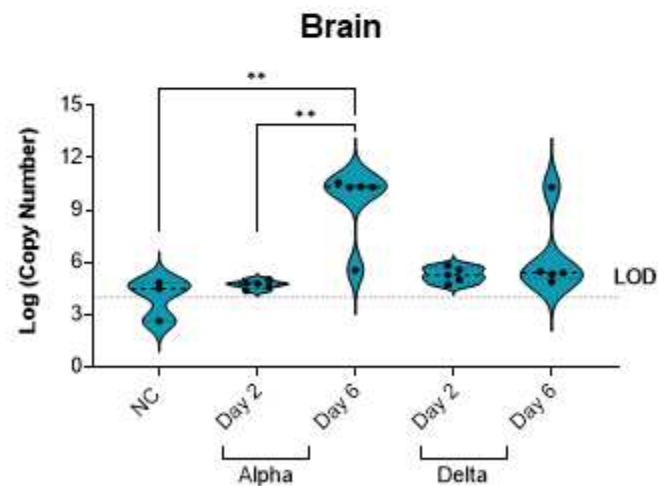
A

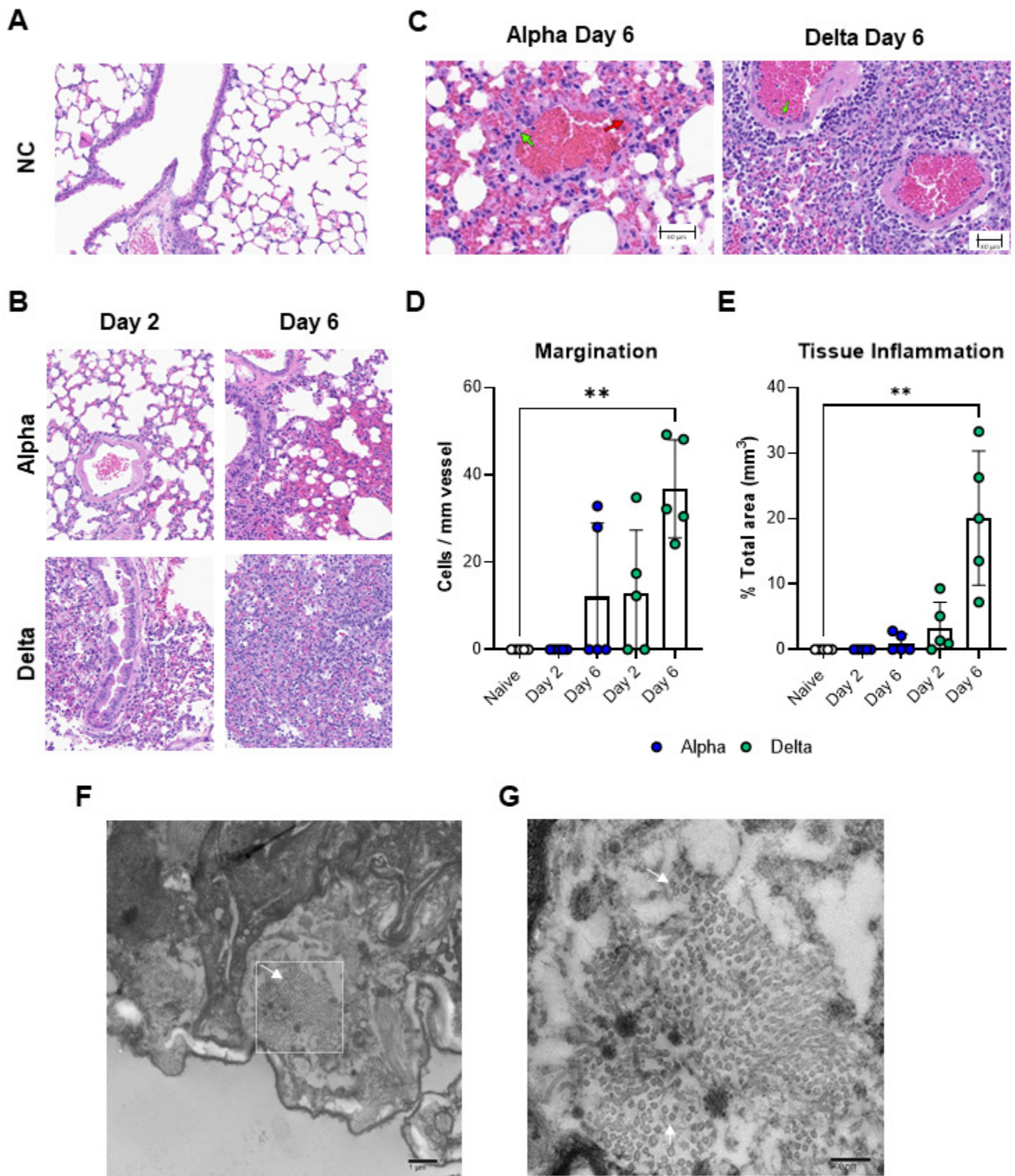


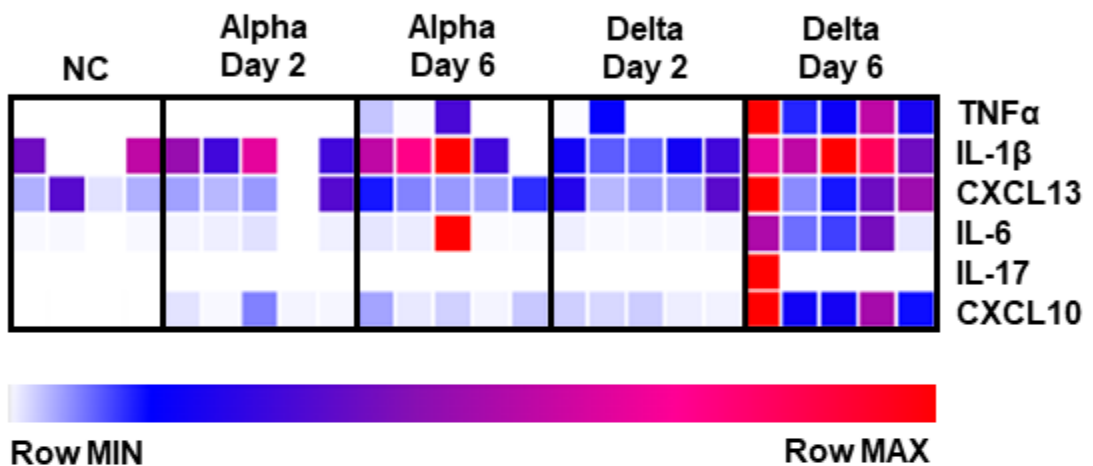
B



C



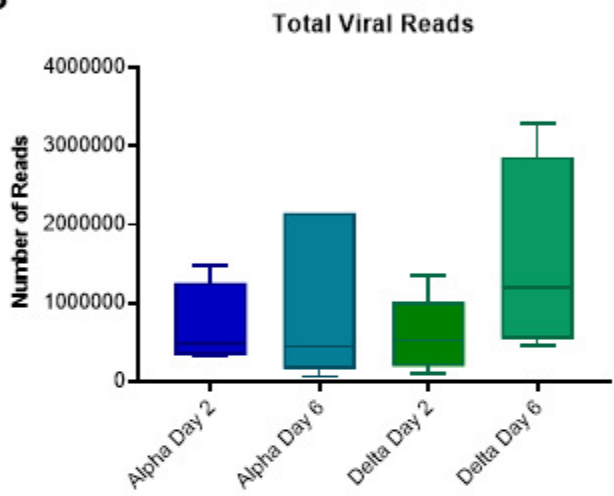




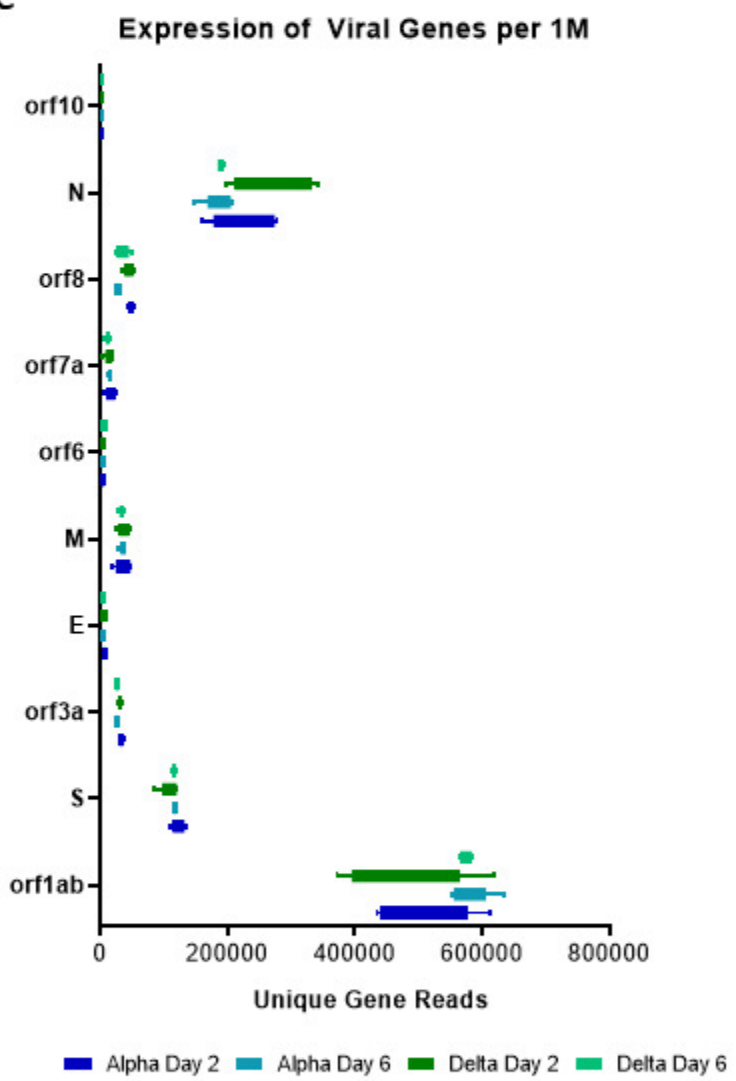
A



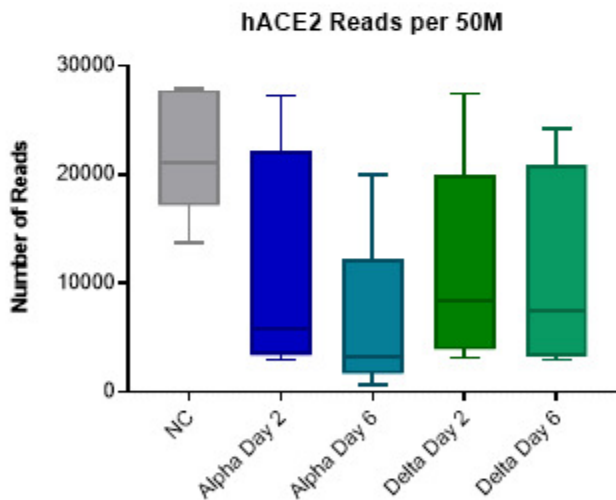
B



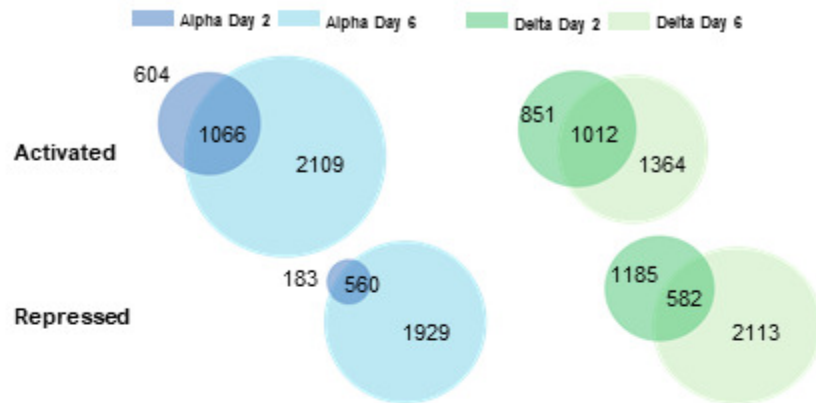
C



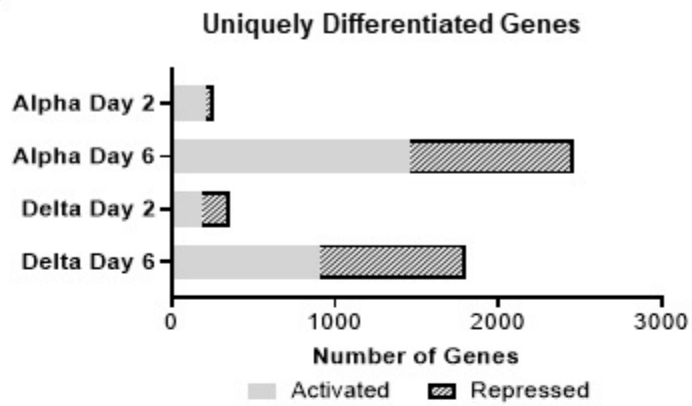
D



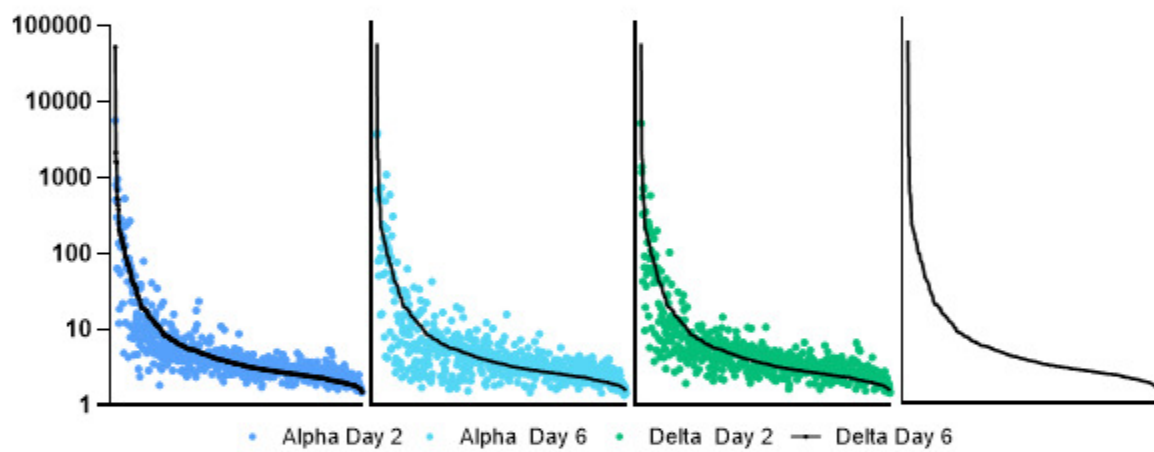
A



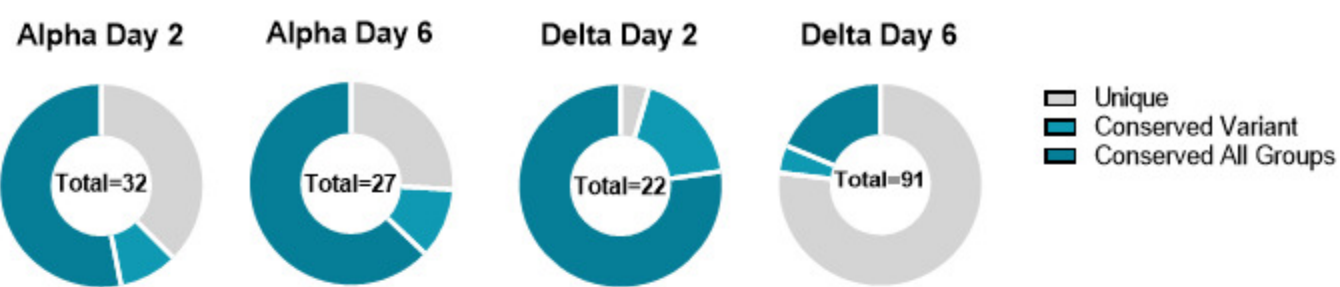
B



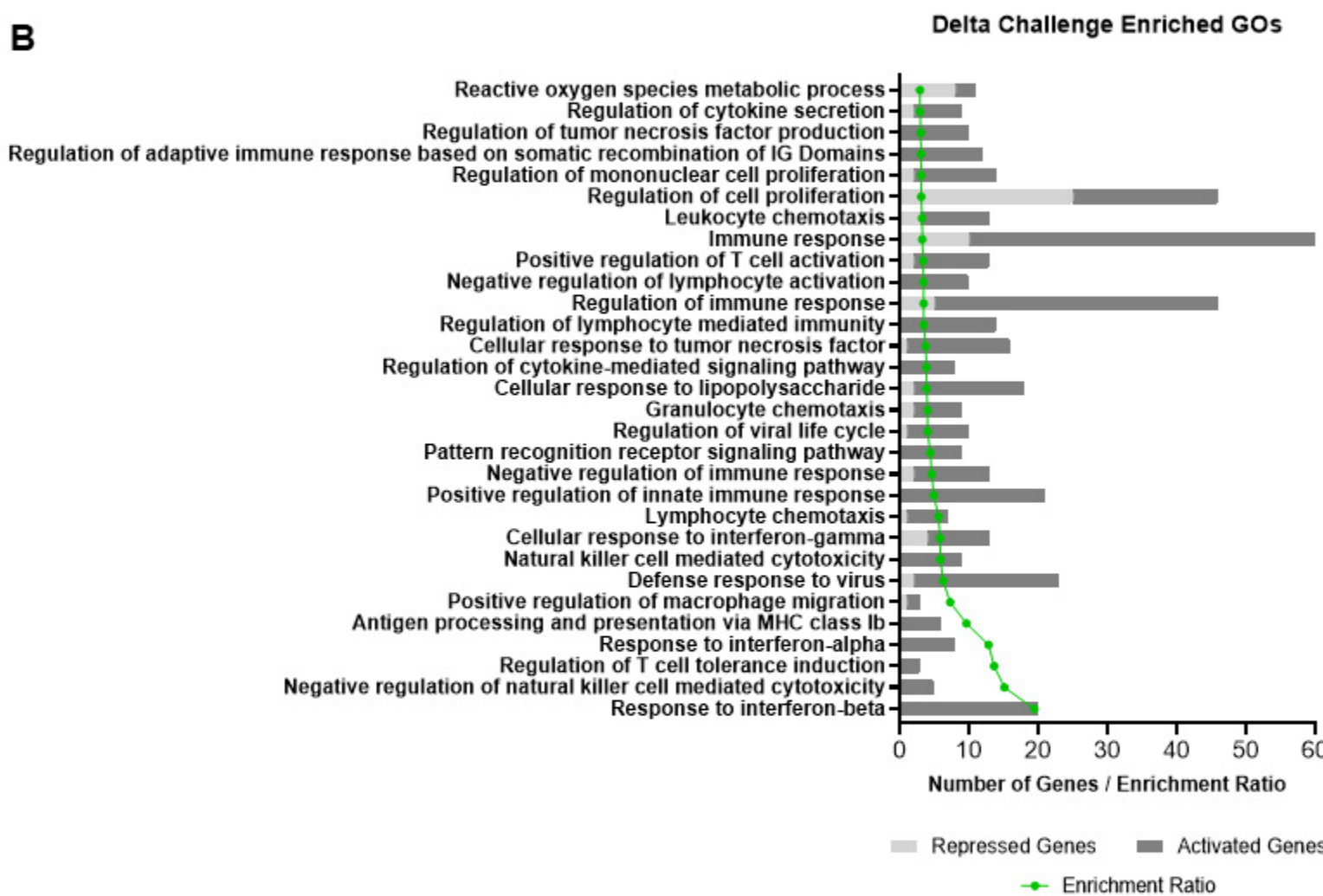
C



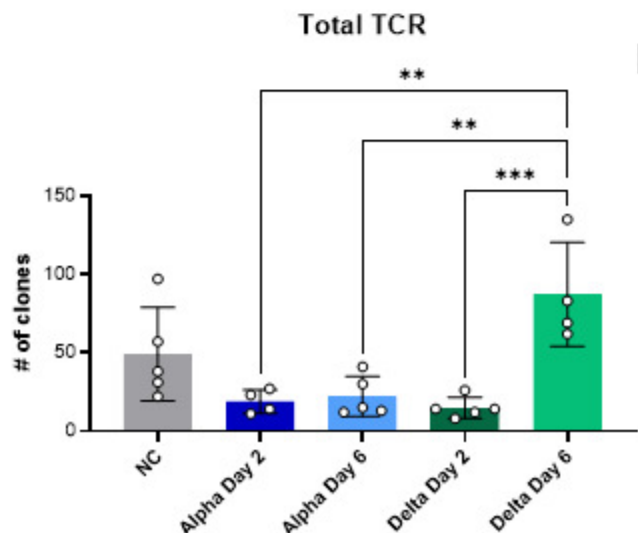
A



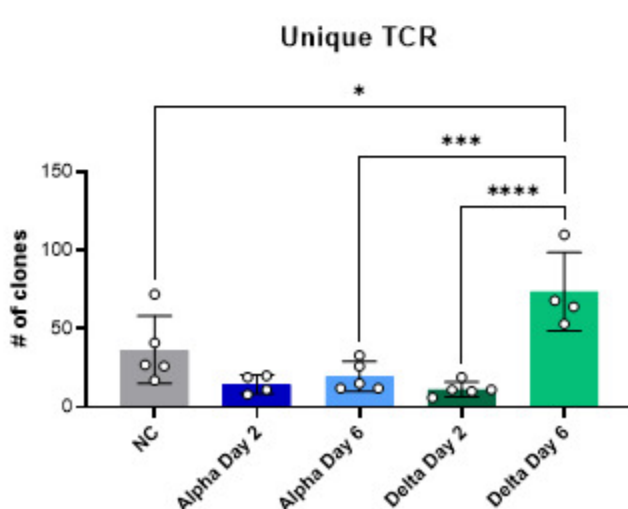
B



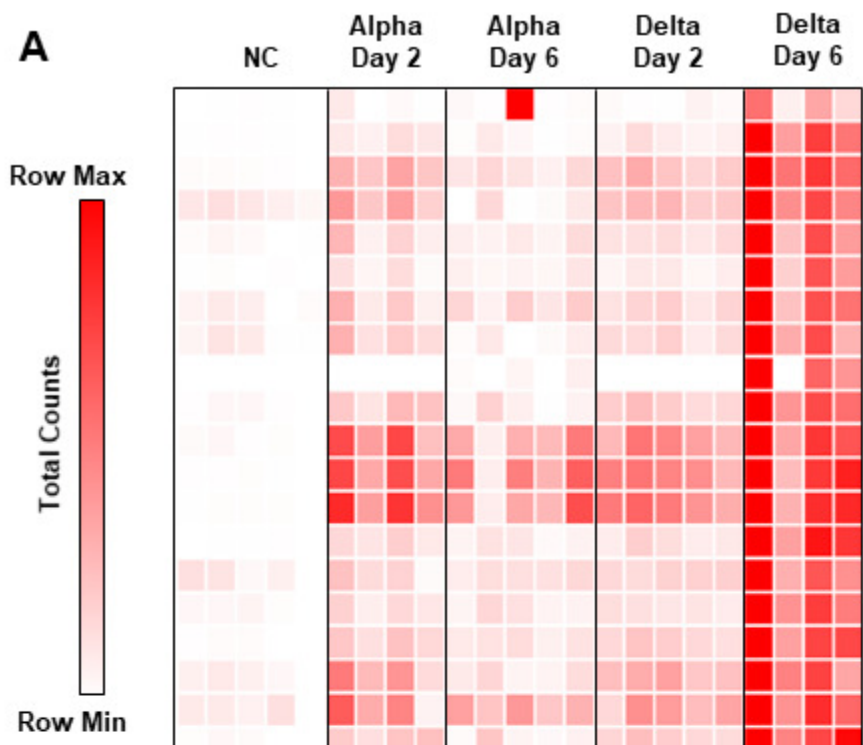
C



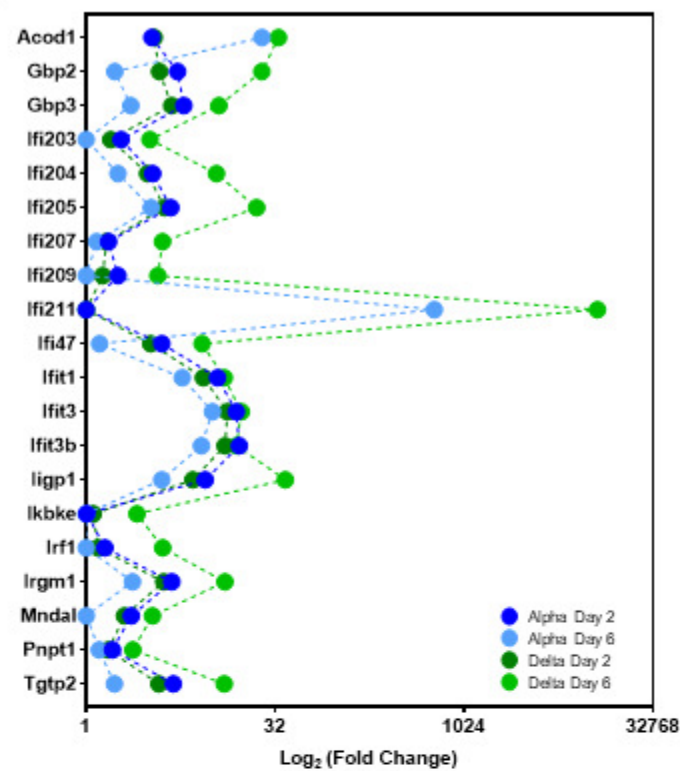
D



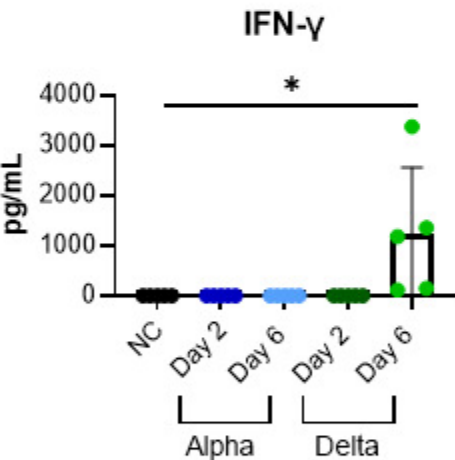
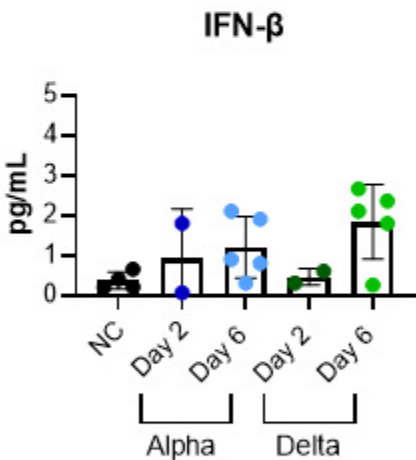
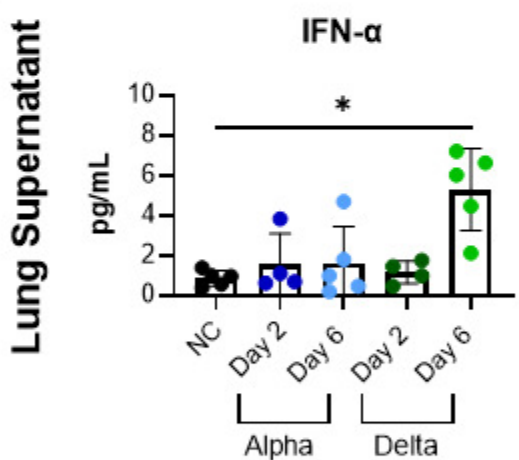
A



B



C



D

